Hindawi
Mathematical Problems in Engineering
Volume 2019, Article ID 1086983, 10 pages
https://doi.org/10.1155/2019/1086983

Research Article

Energy Harvesting from Vehicle Suspension System by Piezoelectric Harvester

Zhen Zhao,[1] Tie Wang,[1,2] Baifu Zhang,[3] and Jinhong Shi[1]

[1]*College of Mechanical and Vehicle Engineering, Taiyuan University of Technology, Taiyuan 030024, China*
[2]*School of Computing and Engineering, University of Huddersfield, Huddersfield HD1 3DH, UK*
[3]*College of Electrical and Power Engineering, Taiyuan University of Technology, Taiyuan 030024, China*

Correspondence should be addressed to Tie Wang; wangtie57@163.com

Received 11 June 2019; Accepted 28 July 2019; Published 15 August 2019

Academic Editor: Georgios I. Giannopoulos

In this paper, a new type of piezoelectric harvester for vehicle suspension systems is designed and presented that addresses the current problems of low energy density, vibration energy dissipation, and reduced energy harvesting efficiency in current technologies. A new dual-mass, two degrees of freedom (2-DOF), suspension dynamic model for the harvester was developed for the inertial mass and the force of the energy conversion component by combining with the piezoelectric power generation model, the rotor dynamics model, and the traditional 2-DOF suspension model. The influence of factors such as vehicle speed, the parameters of the harvester, and road classification on the root mean square (RMS) of the generated electric power is discussed. The results show that the RMS increases with the increase of the speed of the vehicle, the thickness and length of piezoelectric patches and magnetic slabs, and the residual flux density of magnets and road roughness coefficient and with the decrease of the width of piezoelectric patches and magnetic slabs and the space between the stator ring and the rotator ring. In the present research, a power of up to 332.4 W was harvested. The proposed model provides a powerful reference for future studies of energy harvesting from vehicle suspension systems.

1. Introduction

Ongoing energy crises such as oil shortages and problems such as environmental pollution have become great challenges to the automotive industry. As such, interest in recovering energy lost due to vibration during vehicle travel is growing rapidly. The current state of energy harvesting that attempts to convert lost energy into an available form does not focus on the vehicle but on components instead [1, 2]. Energy harvesting technology has significant potential for the current automotive industry by improving vehicle energy efficiency and fuel economy. Similar technologies are widely used in the collection of solar, wind, hydro, thermal, and mechanical energies [3–5]. For vehicles, lost heat, braking energy, and vibration energy are the main targets of energy harvesting [6–8].

The suspension system is an important part of the vehicle chassis and plays a key role in supporting the body and absorbing vibrations caused by rough road [9]. The suspension system energy harvester is the complement for the onboard alternator, and the harvested vibration energy can charge the vehicle battery and provide power for the relevant load [10, 11]. Currently, researchers have conducted numerous studies on energy harvesting based on vehicle suspension systems. When a typical passenger car is driven at a speed of 97 km/h on a good road surface, the potential for harvested power can reach between 100 and 400 W, which is equivalent to a 3% increase in fuel efficiency [12, 13]. The power harvested by the vibration energy device is closely related to the vibration intensity level of the suspension system. Vehicles with large sprung mass, fast driving velocity, and poor driving conditions have a high level of vibration intensity. As a result, the energy harvesting of the suspension system of such vehicles has broader prospects, such as heavy trucks and off-road vehicles [14]. When an off-road vehicle travels on a road of class D at a speed of 80 km/h, the generated electric power can reach as high as 2048 W [6].

Among current energy harvesters, electromagnetic energy harvesters are widely used in vehicle suspension systems for vibration energy harvesting because of higher energy conversion efficiency, compact structure, fast response velocity, and strong controllability [15–17]. Electromagnetic energy harvesters can be primarily divided into two types: linear electromagnetic energy harvesters and rotary electromagnetic energy harvesters [18]. The rotary electromagnetic energy harvester is known to provide higher energy conversion efficiency and a more compact structure than the linear electromagnetic energy harvester [19] by converting linear motion to rotary motion by mechanical or hydraulic transmission [20, 21].

Piezoelectric materials are used in the vibration energy harvesting field because of their associated improved electromechanical coupling effects and higher energy conversion efficiency compared to other materials [22]. The most representative piezoelectric materials are piezoelectric ceramics and piezoelectric polymers [23]. The research reported in the literature shows that piezoelectric materials harvest three times as much energy as electromagnetic materials [24]. Piezoelectric materials have been used to harvest the vibration energy that a person transmits to the ground while walking [25], the energy generated by the differential force between the wearer and the backpack [26], the vibration energy generated by high-rise buildings [27], the energy generated by the longitudinal or transverse wave motion of seawater [28], and the energy generated by the wind [29].

In [30], a piezoelectric energy harvester was used to harvest the vibration energy inside the vehicle suspension system and the tire, and the harvested energy was used to power an embedded wireless sensor. In [31], a new dual-mass piezoelectric energy harvester was designed to collect effective and practical vibration energy from vehicle tires with a maximum power of 42.08 W. In [32], it was demonstrated that the maximum power harvested by a vehicle suspension system can reach 738 W and is affected by road roughness.

The above research shows that vibration energy harvesters have been widely used to harvest vibration energy in various environments. In vehicles, they are primarily used to harvest vibration energy from suspension systems, where hundreds of watts of electrical energy can be generated using electromagnetic or piezoelectric energy harvesters. Both types of harvester have their own associated challenges and disadvantages. Electromagnetic harvesters have a disadvantage of low energy density. Piezoelectric harvesters suffer from problems including vibration energy dissipation and reduced energy harvesting efficiency due to friction between the piezoelectric cantilever and the excitation object within the structure.

In order to address the limitations of the current piezoelectric energy harvesters, this paper designs a new type of ring piezoelectric energy harvester with high energy harvesting efficiency by using magnetic forces. The harvester is composed of a motion conversion component and an energy conversion component. The motion conversion component converts the linear motion between the vehicle body and wheels to rotary motion, and the energy conversion component converts the vibration energy to electric energy. Because of the high frequencies of the magnetic excitation forces applied to the piezoelectric patches and the low friction between the stator and rotator ring, the new harvester proposed in this research has a high energy harvesting efficiency. The factors affecting the RMS of the electric power generated by the piezoelectric energy harvesters are theoretically discussed. The results of this work provide an important reference for future research related to energy harvesting from vehicle suspension.

2. Design and Methods

2.1. Structural Design of the Piezoelectric Harvester. A schematic diagram of the piezoelectric energy harvester and its geometry are shown in Figure 1. The upper end of the harvester is connected to the vehicle body, and the lower end is connected to the wheels. The harvester is connected in parallel with the shock absorber of the original vehicle. The schematic diagram illustrates that the motion conversion component is composed of a ball screw shaft and nut, and the energy conversion component is composed of an outer stator ring and an inner rotator ring. Rectangular magnetic slabs of the same size are uniformly mounted in the circumferential direction on the inner circular surface of the stator ring. The piezoelectric patches are embedded between the magnetic slabs and the stator ring and have the same rectangular dimensions as the magnetic slabs. The rotator ring is connected to the ball screw through a spline structure to achieve torque transmission. On the outer circumference of the rotator ring, a set of magnetic slabs with the exact same size of the piezoelectric patches are placed along the circumferential direction. Through this structure, when the rotator rotates, a periodic magnetic force is generated between the stator ring and the rotator ring, and the magnetic force acts on the piezoelectric patch along the polarization direction, thereby harvesting electrical energy.

In Figure 1, $d = r_1 - r_2$ is the space between the rotator ring and the stator ring, where r_1 is the inner radius of the stator ring and r_2 is the outer radius of the rotator ring. The length of the magnetic slabs and the piezoelectric patches along the axial direction is both given a length, l, and has the same width, w. The thickness of the magnetic slabs is t_m, and the thickness of the piezoelectric patches is t_p. It should be noted that since the width of the magnetic patches is the same as the width of the teeth on the rotator ring, the magnetic force acting on the piezoelectric patches changes continuously and periodically.

2.2. Modelling of Power Generation. In order to analyze the repelling force F_M between two identical rectangular permanent magnets, according to [33], an empirical equation can be expressed as

$$F_M = lwt_m^n B_r |B_d| f(d), \tag{1}$$

where the residual flux density of the magnet is B_r. The relevant values can be obtained from the magnet data table.

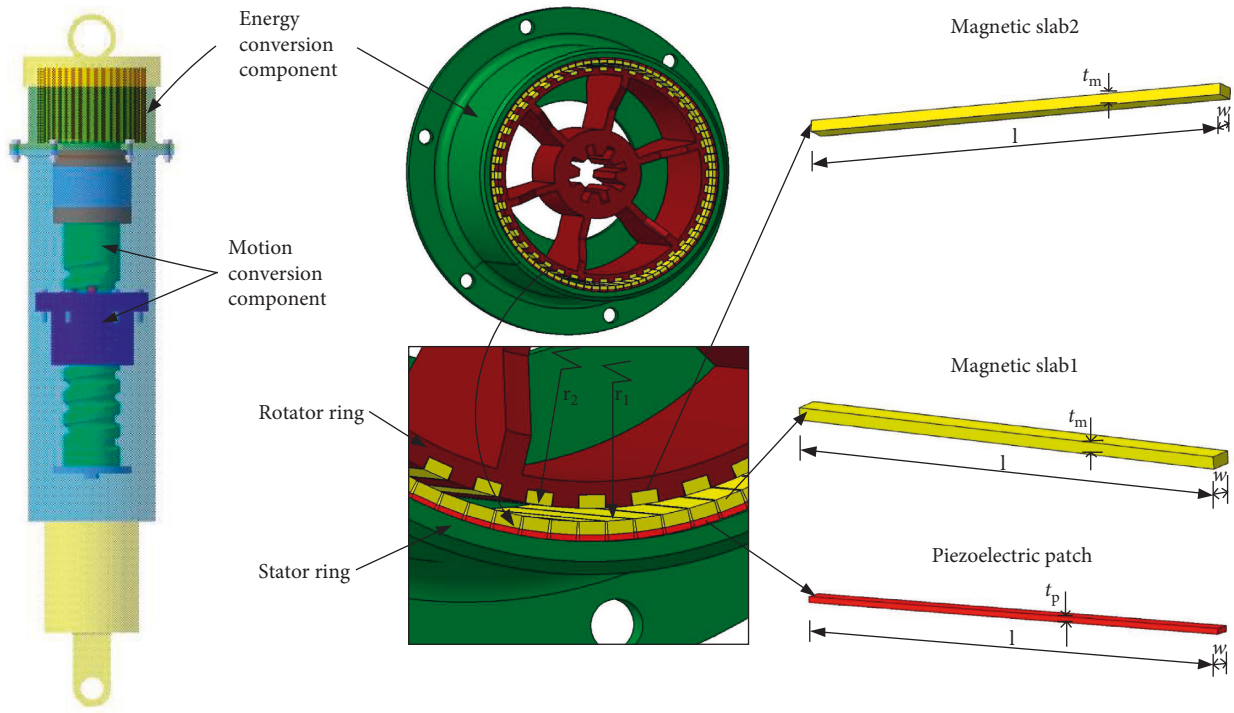

Figure 1: Schematic diagram and geometries of the piezoelectric energy harvester.

The empirical corrective exponent n has a value of 1/3. For the rectangular magnet, the magnitude of the magnetic flux density field is B_d and the empirical function is $f(d)$, which can be used to describe the decay of the repelling force between two magnets. Equations (2) and (3) can be used to calculate B_d and $f(d)$, respectively [34].

$$|B_d| = \frac{B_r}{\pi}\left[\tan^{-1}\left(\frac{lw}{2d\sqrt{4d^2+l^2+w^2}}\right) - \tan^{-1}\left(\frac{lw}{2(t_m+d)\sqrt{4(t_m+d)^2+l^2+w^2}}\right)\right], \quad (2)$$

$$f(d) = \left(1.749 + 1.145e^{(-d/d_0)}\right) \times 10^6\ \mathrm{NT}^{-2}\cdot \mathrm{m}^{(-7/3)}, \quad (3)$$

where $d_0 = 1$ mm.

At time t, the repelling force between the two magnet slabs determines the periodic normal force applied along the poling direction on the piezoelectric patches. Figure 2, a schematic diagram of magnetic force decomposition, shows a frozen instant of the energy conversion component. The magnetic force, F_M, acting on the stator ring magnetic strip can be decomposed into two components: F_{Mx} in the transverse direction and F_{My} in the poling direction of the piezoelectric material axial direction. The rotational angular velocity of the rotator ring is $2\pi n_1$.

When the magnet plates on the rotating ring are at points A and D, the force acting on the piezoelectric ceramic in the polarization direction is $F = 0$. This is because the connection line between the N pole centers of the two magnets is tangent to the rotating magnet, therefore $F_M = 0$. When the magnet plate on the rotating ring rotates to point B (point B is located at any position between A and C), $F = F_{My} = F_M \sin\beta$. When the rotating magnet is at point C, $F = F_M$. Figure 3 shows normal force versus time. It can be assumed that the periodic normal force F applied to the

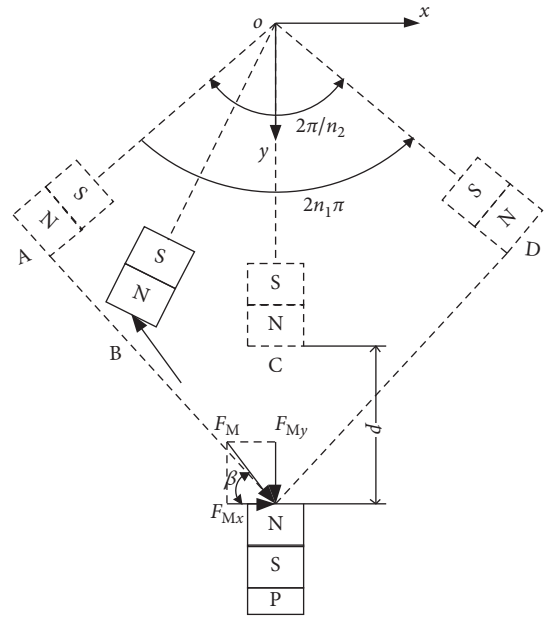

Figure 2: Magnetic force decomposition.

piezoelectric patch changes sinusoidally as the rotator ring rotates.

The period T and normal force F can be written as

$$T = \frac{2(2\pi/n_2)}{2\pi n_1} = \frac{2}{n_1 n_2},$$
$$F = F_M \left|\sin(n_1 n_2 \pi t)\right|, \tag{4}$$

where n_1 is the rotational speed of the rotator ring in cycles per second and $n_2 = \pi r_2/w$ is the number of magnetic slabs embedded on the outer face of the rotator ring. The number of piezoelectric patches mounted on the inner surface of the stator ring is twice the number of magnetic slabs on the rotator ring is therefore equal to $2n_2$. It can be seen that as the width w of the magnetic slabs decreases, the value of $n_2 = \pi r_2/w$ increases, leading to an increase in the excitation frequency on the piezoelectric patches.

The generated periodic charge and voltage on the ith piezoelectric patch can be represented by

$$Q(t) = d_{33} F_M \left|\sin(n_1 n_2 \pi t)\right|,$$
$$V(t) = \frac{d_{33} F_M \left|\sin(n_1 n_2 \pi t)\right|}{C_v}. \tag{5}$$

The RMS of the generated power from time 0 to T is given as

$$P_e^{\text{rms}} = \sqrt{\frac{1}{T}\int_0^t [P_e(t)]^2 dt}, \tag{6}$$

where $P_e(t)$ is the total generated power of all the piezoelectric patches on the stator ring at time t ($0 < t < T$), which is provided as

$$\begin{aligned} P_e(t) &= \sum_{i=1}^{2n_2} \frac{dQ_i(t)}{dt} V_i(t) \\ &= \frac{\sum_{i=1}^{2n_2} d_{33}^2 n_1 n_2 \pi F_M^2 \left|\sin(n_1 n_2 \pi t)\cos(n_1 n_2 \pi t)\right|}{C_v} \\ &= \frac{d_{33}^2 n_1 n_2 \pi F_M^2 \left|\sin(2 n_1 n_2 \pi t)\right|}{C_v}. \end{aligned} \tag{7}$$

To estimate the RMS of the generated electric power, the period, T, can be divided into j time steps with a sufficiently short time interval Δt. As a result, the expression in equation (6) can be rewritten in a discrete form as follows:

$$P_e^{\text{rms}} = \sqrt{\frac{\Delta t}{2(T - \Delta t)} \sum_{i=2}^{j} \left([P_e(t_i)]^2 - [P_e(t_{i-1})]^2 \right)}. \tag{8}$$

2.3. Rotor Dynamics Model. The equations of rotary motion can be used to express the output force of the piezoelectric energy harvester. The rotary motion of the piezoelectric energy harvester can be described in two parts. The first part is the axial to rotary transformation of the ball screw, and the second part is the rotor dynamics of the harvester. Figure 4 shows the rotor dynamics model. The ball screw transforms the axial stroke input into a rotary motion, and then the rotator ring and the ball screw rotate dynamically. In the following derivation, it is assumed that both the rotator ring and the ball screw are rigid and that the backlash, dynamic friction, and torsion of the ball screw can be ignored.

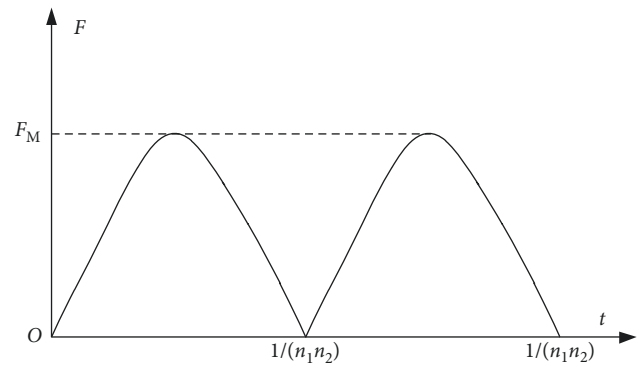

Figure 3: Normal force versus time.

In other words, the following equation should be true during the transformation of the ball screw:

$$\omega = \frac{2\pi \dot{z}}{l_d},$$
$$n_1 = \frac{\dot{z}}{l_d}, \tag{9}$$

where ω is the angular velocity, $\dot{z}$ is the input stroke speed, and l_d is the lead of the ball screw.

The rotor dynamics equation can be described as follows:

$$T = T_p + T_i = T_p + (J_p + J_b)\dot{\omega}. \tag{10}$$

Here, T is output torque of the harvester device, $T_i = (J_p + J_b)\dot{\omega}$ is output inertia torque of the rotating component, T_p is output torque of the energy conversion component, and J_b and J_p are the moment of inertia of ball screw and rotor ring, respectively.

According to the equilibrium of force, the output force in the axial direction is found to be

$$T = \frac{l_d F_z}{2\pi},$$
$$F_z = \frac{2\pi T}{l_d}. \tag{11}$$

Therefore, the axial output force F_z of the energy harvester can be obtained from the following formula:

$$F_z = F_p + F_i = \left(\frac{2\pi}{l_d}\right) T_p + \left(\frac{2\pi}{l_d}\right)^2 (J_p + J_b)\ddot{z}, \tag{12}$$

where F_p is the force of the energy conversion component and $F_i = (2\pi/l_d)^2 (J_p + J_b)\ddot{z}$ is the inertial force generated by the rotating component and is proportional to the acceleration. Therefore, the inertial mass of the energy collection device is defined as

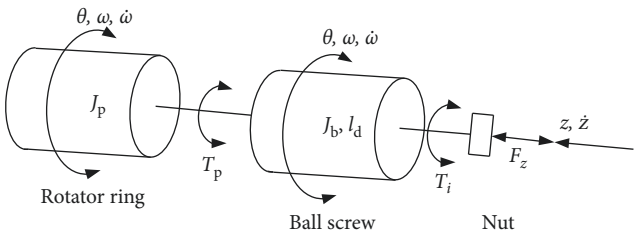

Figure 4: Rotor dynamics model of the piezoelectric energy harvester.

$$m_i = \left(\frac{2\pi}{l_d}\right)^2 \left(J_p + J_b\right). \tag{13}$$

When the input stroke speed $\dot{z}$ is not changed and $F_i = 0$, $F_z = F_p$. In the period of $0 \sim 1/(n_1 n_2)$, the work done by the axial output force F_z of the energy harvester is W_1 and the generated electric energy is W_2.

$$W_1 = F_p \dot{z} \left(\frac{1}{n_1 n_2}\right). \tag{14}$$

W_2 is available from the following equation:

$$W_2 = \int_0^{(1/n_1 n_2)} \frac{d_{33}^2 n_1 n_2 \pi F_M^2 \left|\sin\left(2n_1 n_2 \pi t\right)\right|}{C_v} dt = \frac{2d_{33}^2 n_2 F_M^2}{C_v}. \tag{15}$$

Because $W_1 = W_2$, equations (14) and (15) can be combined to yield

$$F_p = \frac{2d_{33}^2 F_M^2 n_2^2}{C_v l_d}. \tag{16}$$

The above equation shows that F_p is not affected by the input stroke speed $\dot{z}$ and is inversely proportional to l_d.

2.4. Dual-Mass 2-DOF Suspension Dynamic Model. Figure 5 shows the dual-mass 2-DOF suspension dynamic model, where m_i is the inertial mass, F_p is the force of the energy conversion component, m_b is the body mass, m_t is the wheel mass, k is the stiffness of the spring, k_t is the tire stiffness, and c is the damping coefficient of the shock absorber. The coordinates of vertical displacement between the wheels and body are z_t and z_b, respectively. When the origin of coordinates is selected at their respective equilibrium positions, the equations of motion are established below according to Newton's second law:

$$\begin{cases} m_b \ddot{z}_b + m_i\left(\ddot{z}_b - \ddot{z}_t\right) + c\left(\dot{z}_b - \dot{z}_t\right) \\ \quad + k\left(z_b - z_t\right) + F_p \mathrm{sgn}\left(\dot{z}_b - \dot{z}_t\right) = 0, \\ m_t \ddot{z}_t + m_i\left(\ddot{z}_t - \ddot{z}_b\right) + c\left(\dot{z}_t - \dot{z}_b\right) + k\left(z_t - z_b\right) \\ \quad + k_t\left(z_t - q(t)\right) + F_p \mathrm{sgn}\left(\dot{z}_t - \dot{z}_b\right) = 0, \end{cases} \tag{17}$$

where $q(t)$ is the uneven road surface which can be obtained using the following equation:

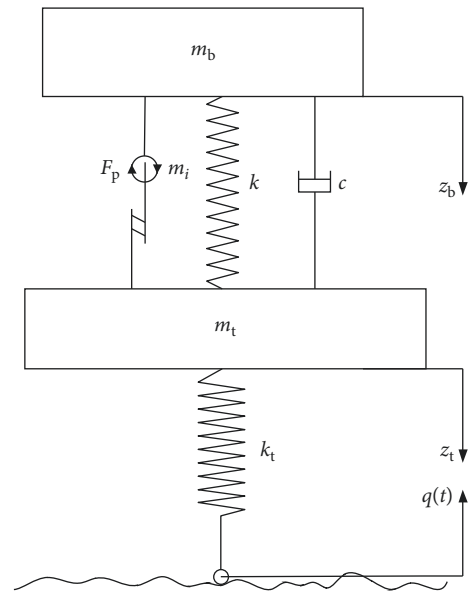

Figure 5: Dual-mass 2-DOF suspension dynamic model.

$$\dot{q}(t) = -2\pi n_{00} v q(t) + 2\pi n_0 \sqrt{G_q(n_0) v} W(t), \tag{18}$$

where $n_{00} = 0.011\ \mathrm{m}^{-1}$ is a minimal boundary frequency, $n_0 = 0.1\ \mathrm{m}^{-1}$ is the reference spatial frequency, $G_q(n_0)$ is the roughness coefficient in m^3, $W(t)$ is the Gaussian white noise with a mean of zero, and v is the vehicle speed in m/s.

3. Simulation Results and Discussions

In this section, the characteristics of the power generated by the newly designed piezoelectric energy harvester are studied. The analysis focuses on the impact of several key parameters on the generated power. These are the road surface class, the driving speed of the vehicle, the space between the stator ring and the rotator ring, the residual flux density of the magnet, and the geometrical dimensions (length, width, and thickness) of the piezoelectric patches and the magnetic slabs. Tables 1 and 2 list the relevant material properties and dimensions of the piezoelectric harvester and the parameters of the quarter-car model in the simulations. Three classes of road roughness, namely, B, C, and D, were selected and are given in Table 3. The stator ring and the rotator ring, which are the main structures of the harvester, are made of aluminum. The material of the piezoelectric patches is PZT-4 (lead zirconate titanate). N5311 (neodymium iron boron) is the material for magnetic slabs.

Figure 6 has three curves to depict the relationship between the RMS of the generated power and the road roughness class and the speed of the vehicle. The dimensions of the harvester in these simulations were set to $t_m = 0.01$ m, $t_p = 0.01$ m, $l = 0.1$ m, $w = 0.002$ m, $d = 0.0005$ m, $r_2 = 0.05$ m, and $B_r = 1.5$ T. This figure shows that RMS power generation is related to the road roughness class when the vehicle is traveling at the same speed on different road roughness classes. On a road of class D, the RMS has the maximum value, followed by the value on a road of class C, and the

Table 1: Material properties and dimensions of the piezoelectric ring generator.

r_2 (m)	d (m)	B_r (T)	t_m (m)	t_p (m)	w (m)	l (m)	d_{33} (CN^{-1})
0.05	0.0005~0.005	0.5~1.5	0.001~0.01	0.001~0.01	0.002~0.02	0.01~0.1	6.4 e–10
C_v (nF)	0.375 for the piezoelectric patch with the geometry of w = 0.01 m, l = 0.01 m, and t_p = 0.0001 m						

Table 2: Parameters of the quarter-vehicle model.

m_t (kg)	m_b (kg)	m_i (kg)	c (kN · s/m)	k (kN/m)	k_t (kN/m)	l_d (m)
30	362	5.3	1.4	20.1	182.1	0.01

Table 3: Road roughness coefficient $G_q(n_0)$ (m^3) classified by ISO/TC108/SC2N67.

Road class	A	B	C	D	E	F	G	H
$G_q(n_0)$ ($\times 10^{-6}$)	16	64	256	1024	4096	16,384	66,536	262,144

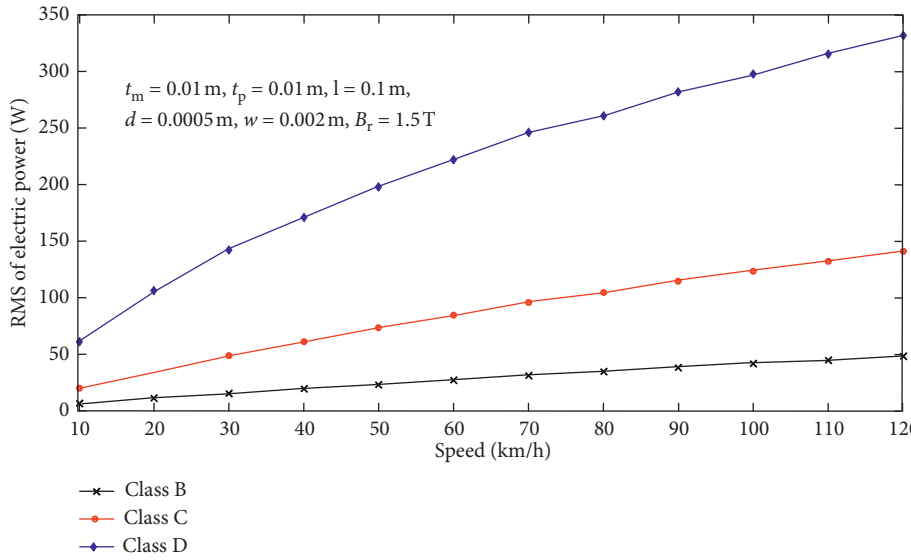

Figure 6: RMS of the electric power versus the driving speed of the vehicle.

minimum is on a road of class B. On the road of class D, when the vehicle speed was increased from 10 km/h to 120 km/h, the corresponding RMS of the generated electric power increased from 61.6 to 332.4 W. However, the relative increase in the amplitude of RMS decreases as the speed increases. Based on these results, it can be concluded that a faster driving speed and worse road roughness class lead to a larger excitation frequency of the magnetic force applied to the piezoelectric patches which subsequently leads to a corresponding increase in the RMS electric power generation.

Figure 7 shows the effect of the changes in space between the stator ring and the rotator ring, d, on the RMS of the generated electric power. The parameters of the energy harvester during the simulations were set to $t_m = t_p = 0.01$ m, $l = 0.1$ m, $w = 0.002$ m, $r_2 = 0.05$ m, $B_r = 1.5$ T, and $v = 80$ km/h, and the road of class D was used. From the simulation results, it can be found that the RMS decreases nonlinearly with an increase in the space between the stator ring and the rotator ring. When the space between the stator ring and the rotator ring was decreased from 0.005 to 0.0005 m, the RMS increased significantly from 2.7 to 261.1 W. It is clear that the magnetic force acting on the piezoelectric patches is larger due to the narrower space between the stator ring and the rotor ring, causing the generated power to increase.

When the residual flux density of the magnet was changed from 0.5 to 1.5 T, the RMS of the generated electric power variation of the generated power is shown in Figure 8. The geometric parameters of the harvester in the simulation were set to $t_m = t_p = 0.01$ m, $l = 0.1$ m, $w = 0.002$ m, $r_2 = 0.05$ m, $d = 0.001$ m, and $v = 80$ km/h, and the road of class D was used. It can be seen from the trend of the curve in the figure that the RMS is exponentially proportional to the residual flux density of the magnet. When the residual flux density was increased from 0.5 to 1.5 T, the RMS increased sharply from 1.4 to 109.1 W. Therefore, it is clear that a slight

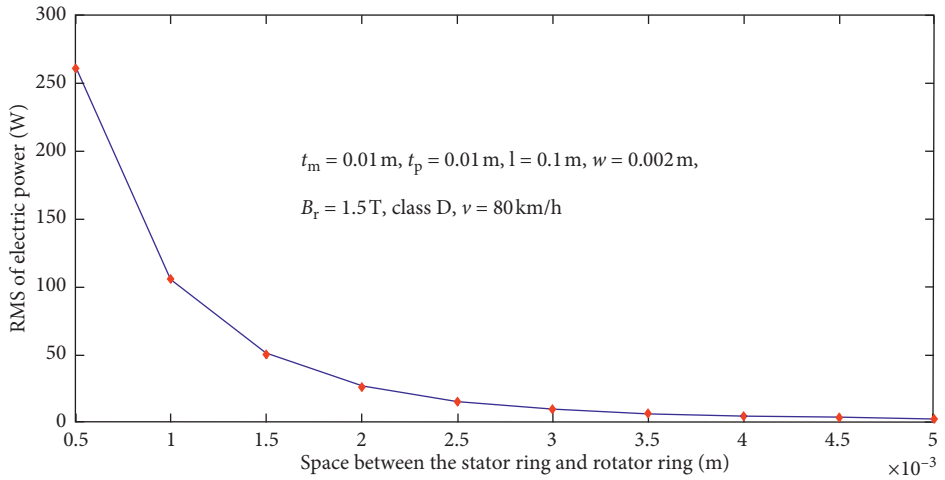

Figure 7: RMS of the electric power versus the space between the stator ring and the rotator ring.

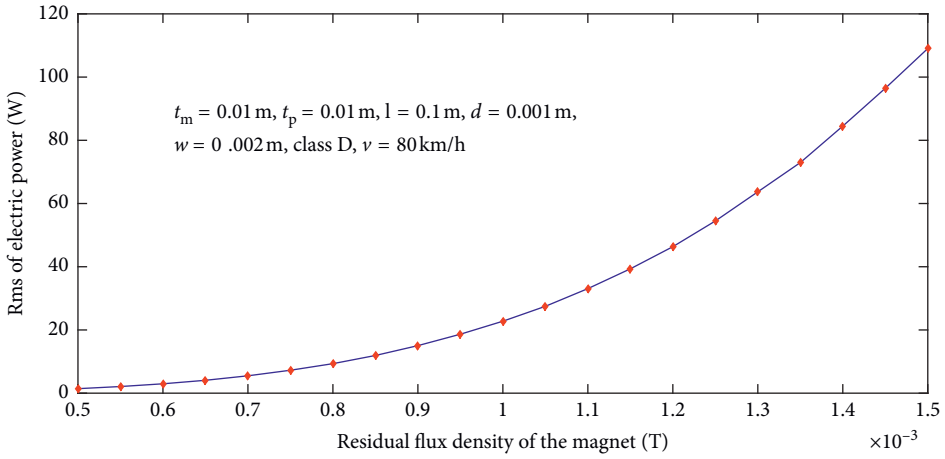

Figure 8: RMS of the electric power versus the residual flux density of the magnet.

increase in the residual flux density of the magnet can result in a significant increase in the RMS power generation.

The effect of the thicknesses of the piezoelectric patches t_p and the magnetic slabs t_m on the RMS of the generated electric power are demonstrated in Figure 9. Before the simulation, the relevant parameters of the harvester were set to $l = 0.1$ m, $w = 0.002$ m, $d = 0.001$ m, $r_2 = 0.05$ m, $B_r = 1.5$ T, and $v = 80$ km/h, and the road of class D was used. By examining the curves in the figure, it can be found that the RMS increases linearly with the thickness of the piezoelectric patches and the thickness of the magnetic slabs. When the thickness was increased from 0.001 m to 0.01 m, the RMS increases significantly from 0.53 to 109.1 W. Thus, it can be concluded that increasing the thicknesses of the piezoelectric patches and the magnetic slabs has a positive effect on the efficiency of the harvester.

Figure 10 shows the effect of the width, w, and the length, l, of the piezoelectric patches and the magnetic slabs on the RMS of the generated electric power. For this simulation the geometric parameters were set to $l = 0.01$~0.1 m, $w = 0.002$~0.02 m, $t_m = t_p = 0.01$ m, $r_2 = 0.05$ m, $B_r = 1.5$ T, and $v = 80$ km/h, and the road of class D was used. By analyzing the simulation results, the following conclusions can be made. First, the relationship between the RMS and the width of the magnetic slab w is discussed. Equations (6) and (7) show a nonlinear increase of the RMS with a decrease in the width of the magnetic slab w. This is primarily because decreasing the width subsequently increases the number of magnetic slabs $n_2 = \pi r_2 / w$ embedded on the rotator ring which causes the excitation frequency of the magnetic force $\omega = n_1 n_2 \pi$ acting on the piezoelectric patches to increase. Eventually, this increase in frequency promotes a rapid increase in the RMS of the generated electric power. Secondly, the RMS value increases approximately linearly with an increase in the length of the magnetic slab l. When the width was set to $w = 0.002$ m and the length of the magnetic slab l was increased from 0.01 m to 0.1 m, the RMS of the generated power increased from 12.7 to 109.1 W.

Due to the limitations of the installation space of the energy harvester in the vehicle, its external dimensions are fixed. The present work can be used to provide guidance for selecting the appropriate width and thickness of the piezoelectric patches and magnetic slabs to

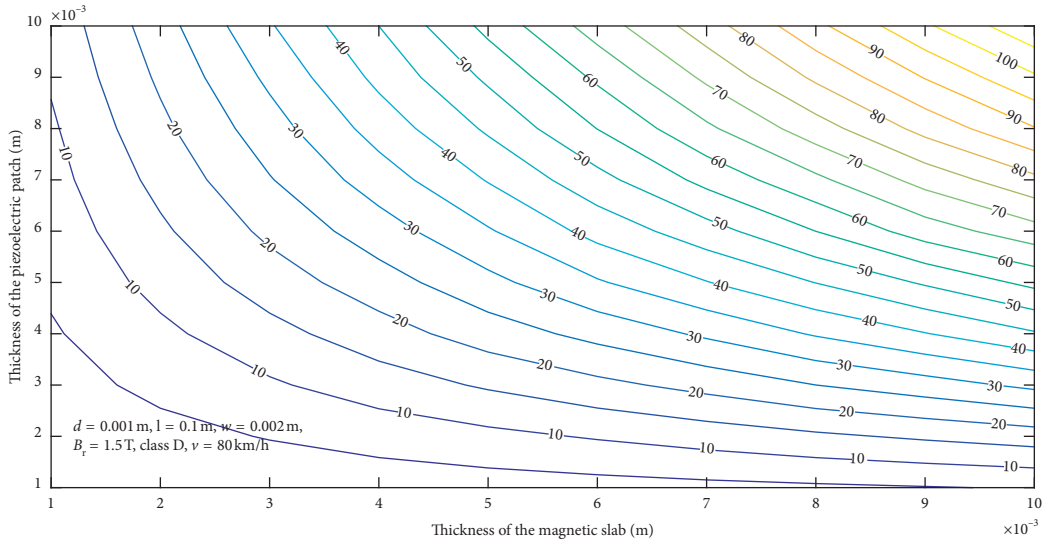

Figure 9: RMS of the electric power versus the thicknesses of the magnetic slab and the piezoelectric patch.

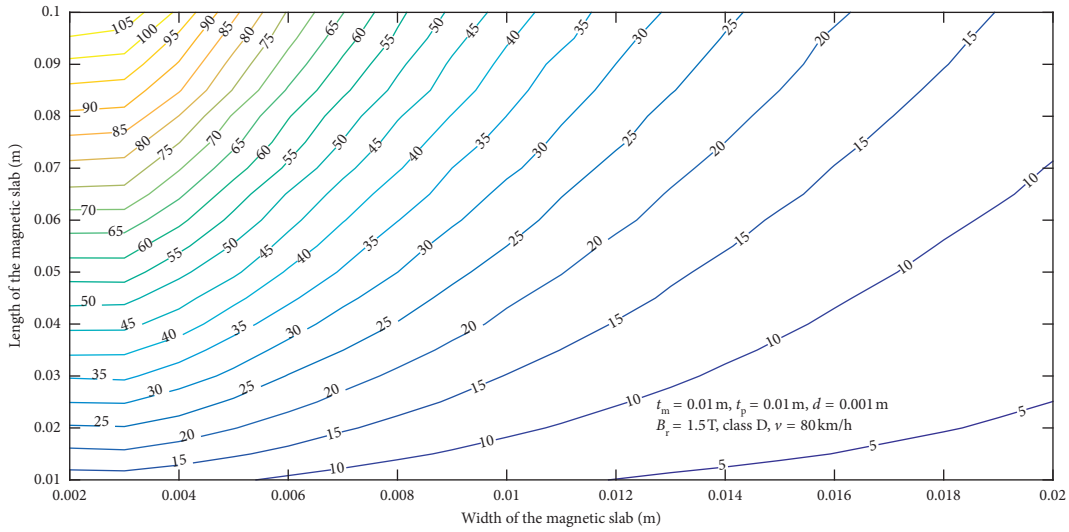

Figure 10: RMS of the electric power versus the width and the length of the magnetic slab.

achieve maximum power generation. When the length was fixed at $l = 0.1$ m and the width of the magnetic slab w was increased from 0.002 m to 0.02 m, the RMS of the generated electric power decreased from 109.1 W to 13.5 W. In summary, the RMS is proportional to the length of the magnetic slab, l, and inversely proportional to its width w. It should be noted that the outer radius of the rotator ring was set to 0.05 m during all of the simulation calculations of the RMS of the generated electric power. Through examining the present simulation results, it is found that the novel piezoelectric energy harvester design in this paper can generate hundreds of watts (W) of electric power which can be used to power automotive electrical equipment such as lamps and air-conditioning systems. It is also possible to store this energy in a battery or supercapacitor for use as needed.

4. Conclusions

A new piezoelectric harvester device with high efficiency was designed for harvesting vibration energy from the suspension system during vehicle travel. A corresponding mathematical model was developed to calculate the output charge and voltage from the magnetically excited piezoelectric piece. This dual-mass 2-DOF suspension dynamics model was established by introducing inertial mass and an applied force to the energy conversion components. Numerical simulation results from the present piezoelectric harvester model show that the RMS of the generated electric power increases with an increase in the length and thicknesses of the piezoelectric patch and the magnetic slab, the driving speed of the vehicle, the residual flux density of the magnet, and the road roughness. In addition, the RMS increased with

a decrease in the space between the stator ring and the rotator ring and the width of the piezoelectric patch and the magnetic slab. It was found that a practical configuration of the present design was shown to provide a power up to 332.4 W. The research presented in this work provides a new method of efficient and practical energy harvesting from suspension systems, thereby improving the energy efficiency of the vehicle.

Data Availability

The .mat data used to support the findings of this study are available from the corresponding author upon request.

Conflicts of Interest

The authors declared no potential conflicts of interest with respect to the research, authorship, and publication of this article.

Acknowledgments

This work was supported by the Science and Technology Projects of Shanxi under 20181102006.

References

[1] C. Ergun, S. Yilmaz, E. Ozdemir, O. Gul, and O. Kalenderli, "Piezoelectric materials and application areas," in *Proceedings of the Denizli International Materials Conference*, Pamukkale, Turkey, November 2006.

[2] X. Han, W. Zeng, and Z. Han, "Investigation of the comprehensive performance of turbine stator cascades with heating endwall fences," *Energy*, vol. 174, pp. 1188–1199, 2019.

[3] M. K. A. Ali, H. Xianjun, M. A. A. Abdelkareem, M. Gulzar, and A. H. Elsheikh, "Novel approach of the graphene nanolubricant for energy saving via anti-friction/wear in automobile engines," *Tribology International*, vol. 124, pp. 209–229, 2018.

[4] H. Wang, A. Jasim, and X. Chen, "Energy harvesting technologies in roadway and bridge for different applications—a comprehensive review," *Applied Energy*, vol. 212, pp. 1083–1094, 2018.

[5] M. K. A. Ali, P. Fuming, H. A. Younus et al., "Fuel economy in gasoline engines using Al_2O_3/TiO_2 nanomaterials as nanolubricant additives," *Applied Energy*, vol. 211, pp. 461–478, 2018.

[6] Y. Zhang, K. Guo, D. Wang, C. Chen, and X. Li, "Energy conversion mechanism and regenerative potential of vehicle suspensions," *Energy*, vol. 119, pp. 961–970, 2017.

[7] L. Pugi, M. Pagliai, A. Nocentini, G. Lutzemberger, and A. Pretto, "Design of a hydraulic servo-actuation fed by a regenerative braking system," *Applied Energy*, vol. 187, pp. 96–115, 2017.

[8] C. Wei and X. Jing, "A comprehensive review on vibration energy harvesting: modelling and realization," *Renewable and Sustainable Energy Reviews*, vol. 74, pp. 1–18, 2017.

[9] B. Heißing and M. Ersoy, *Chassis Handbook (Fundamentals, Driving Dynamics, Components, Mechatronics, Perspectives)*, Mercedes Druck, Berlin, Germany, 2011.

[10] Z. Zhang, X. Zhang, W. Chen et al., "A high-efficiency energy regenerative shock absorber using supercapacitors for renewable energy applications in range extended electric vehicle," *Applied Energy*, vol. 178, pp. 177–188, 2016.

[11] Z. Zhang, X. Zhang, Y. Rasim, C. Wang, B. Du, and Y. Yuan, "Design, modelling and practical tests on a high-voltage kinetic energy harvesting (EH) system for a renewable road tunnel based on linear alternators," *Applied Energy*, vol. 164, pp. 152–161, 2016.

[12] L. Zuo and P. S. Zhang, "Energy harvesting, ride comfort, and road handling of regenerative vehicle suspensions," *Journal of Vibration and Acoustics*, vol. 135, no. 1, article 011002, 2013.

[13] J. Fairbanks, "Vehicular thermo electrics: the new green technology," in *Proceedings of the Thermo electric applications workshop*, Coronado, CA, USA, January 2011.

[14] M. A. A. Abdelkareem, L. Xu, M. K. A. Ali et al., "Vibration energy harvesting in automotive suspension system: a detailed review," *Applied Energy*, vol. 229, pp. 672–699, 2018.

[15] P. Li, L. Zuo, J. Lu, and L. Xu, "Electromagnetic regenerative suspension system for ground vehicles," in *Proceedings of the IEEE International Conference on Systems, Man, and Cybernetics (SMC)*, pp. 2513–2518, San Diego, CA, USA, October 2014.

[16] I. L. Cassidy, J. T. Scruggs, S. Behrens, and H. P. Gavin, "Design and experimental characterization of an electromagnetic transducer for large-scale vibratory energy harvesting applications," *Journal of Intelligent Material Systems and Structures*, vol. 22, no. 17, pp. 2009–2024, 2011.

[17] R. Zhang, X. Wang, and Z. Liu, "A novel regenerative shock absorber with a speed doubling mechanism and its Monte Carlo simulation," *Journal of Sound and Vibration*, vol. 417, pp. 260–276, 2018.

[18] P. S. Zhang, "Design of electromagnetic shock absorbers for energy harvesting from vehicle suspensions," Dissertation, Stony Brook University, Stony Brook, NY, USA, 2010.

[19] P. Li and L. Zuo, "Assessment of vehicle performances with energy-harvesting shock absorbers," *SAE International Journal of Passenger Cars—Mechanical Systems*, vol. 6, no. 1, pp. 18–27, 2013.

[20] T. Lin, Y. Pan, S. Chen, and L. Zuo, "Modeling and field testing of an electromagnetic energy harvester for rail tracks with anchorless mounting," *Applied Energy*, vol. 213, pp. 219–226, 2018.

[21] C. Li and P. W. Tse, "Fabrication and testing of an energy-harvesting hydraulic damper," *Smart Materials and Structures*, vol. 22, no. 6, article 065024, 2013.

[22] S. Shevtsov and M. Flek, "Random vibration energy harvesting by piezoelectric stack charging the battery," *Procedia Engineering*, vol. 144, pp. 645–652, 2016.

[23] H. S. Kim, J.-H. Kim, and J. Kim, "A review of piezoelectric energy harvesting based on vibration," *International Journal of Precision Engineering and Manufacturing*, vol. 12, no. 6, pp. 1129–1141, 2011.

[24] S. Priya, "Advances in energy harvesting using low profile piezoelectric transducers," *Journal of Electroceramics*, vol. 19, no. 1, pp. 167–184, 2007.

[25] A. C. Turkmen and C. Celik, "Energy harvesting with the piezoelectric material integrated shoe," *Energy*, vol. 150, pp. 556–564, 2018.

[26] J. Granstrom, J. Feenstra, H. A. Sodano, and K. Farinholt, "Energy harvesting from a backpack instrumented with piezoelectric shoulder straps," *Smart Materials and Structures*, vol. 16, no. 5, pp. 1810–1820, 2007.

[27] X. D. Xie, Q. Wang, and S. J. Wang, "Energy harvesting from high-rise buildings by a piezoelectric harvester device," *Energy*, vol. 93, no. 2, pp. 1345–1352, 2015.
[28] X. D. Xie, Q. Wang, and N. Wu, "Potential of a piezoelectric energy harvester from sea waves," *Journal of Sound and Vibration*, vol. 333, no. 5, pp. 1421–1429, 2014.
[29] N. Wu, Q. Wang, and X. D. Xie, "Wind energy harvesting with a piezoelectric harvester," *Smart Materials and Structures*, vol. 22, no. 9, article 095023, 2013.
[30] B. Lafarge, C. Delebarre, S. Grondel, O. Curea, and A. Hacala, "Analysis and optimization of a piezoelectric harvester on a car damper," *Physics Procedia*, vol. 70, pp. 970–973, 2015.
[31] X. Xie and Q. Wang, "A mathematical model for piezoelectric ring energy harvesting technology from vehicle tires," *International Journal of Engineering Science*, vol. 94, pp. 113–127, 2015.
[32] X. D. Xie and Q. Wang, "Energy harvesting from a vehicle suspension system," *Energy*, vol. 86, pp. 385–392, 2015.
[33] kjmagnetics.com, Pipersville, PA: The Original K&J Magnet Calculator, 2018, https://www.kjmagnetics.com/calculator.asp/.
[34] W. Al-Ashtari, M. Hunstig, T. Hemsel, and W. Sextro, "Frequency tuning of piezoelectric energy harvesters by magnetic force," *Smart Materials and Structures*, vol. 21, no. 3, article 035019, 2012.